

Histogram Layers for Texture Analysis

Joshua Peeples Weihuang Xu Alina Zare

Department of Electrical and Computer Engineering, University of Florida
Gainesville, FL, 32611

{jpeeples, weihuang.xu, azare}@ufl.edu

Abstract

We present a histogram layer for artificial neural networks (ANNs). An essential aspect of texture analysis is the extraction of features that describe the distribution of values in local spatial regions. The proposed histogram layer leverages the spatial distribution of features for texture analysis and parameters for the layer are estimated during backpropagation. We compare our method with state-of-the-art texture encoding methods such as the Deep Encoding Network (DEP) [39] and Deep Texture Encoding Network (DeepTEN) [42] on three texture datasets: (1) the Describable Texture Dataset (DTD) [10]; (2) an extension of the ground terrain in outdoor scenes (GTOS-mobile) [39]; (3) and a subset of the Materials in Context (MINC-2500) dataset [5]. Results indicate that the inclusion of the proposed histogram layer improves performance. The source code for the histogram layer is publicly available¹.

1. Introduction

Texture analysis is a crucial component in many applications including autonomous vehicles [12], automated medical diagnosis [7], and explosive hazard detection [2]. The concept of texture is easily discernible for humans, but there is no agreed definition within the computer vision community [35, 20]. Generally, variations in the definition of texture arise of differences in the application being studied (i.e., texture characteristics that are more informative vary across application areas) [35, 20]. Yet, most agree that one common component of texture analysis relies on characterizing the spatial distribution of intensity and/or feature values.

A number of handcrafted features have been developed with successful application to texture-dependent computer vision problems. However, the process to design these features can be difficult. Feature engineering is an expensive

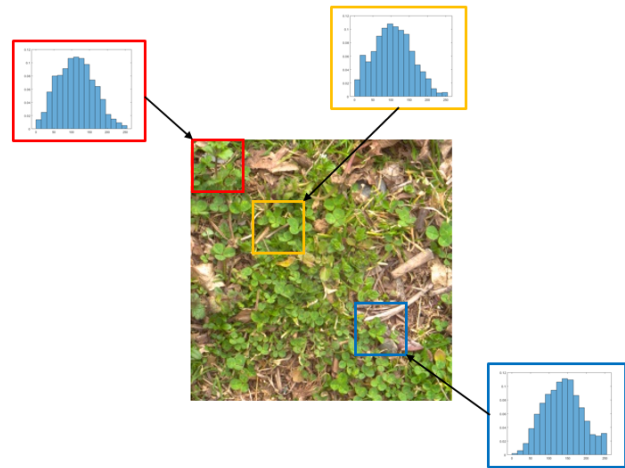


Figure 1: This is an example image of grass from GTOS-mobile [39]. The image contains other textures and not only grass. Local histograms can distinguish portions of the image containing pure grass (top two histograms) or a mixture of other textures (bottom histogram). Integrating a histogram layer in deep neural networks will assist in estimating the data distribution to improve texture analysis.

process in terms of labor, computation, and time and often required significant domain knowledge and expertise. Additionally, these features often rely on empirically determining the best parameters for each descriptor resulting in an increase of computation and time. For example, histogram-based features such as histogram of oriented gradients (HOG) [13] and local binary patterns (LBP) [29] have been extensively studied and used in texture-based applications [25, 14, 28, 40]. In both HOG and LBP feature sets, spatial distributions of feature values are used to characterize and distinguish textures. Furthermore, the distributions are summarized using histograms.

In recent work, these handcrafted approaches are often substituted with deep learning to address some of the issues associated with designing features. Deep learning has

¹Location of code will be posted soon

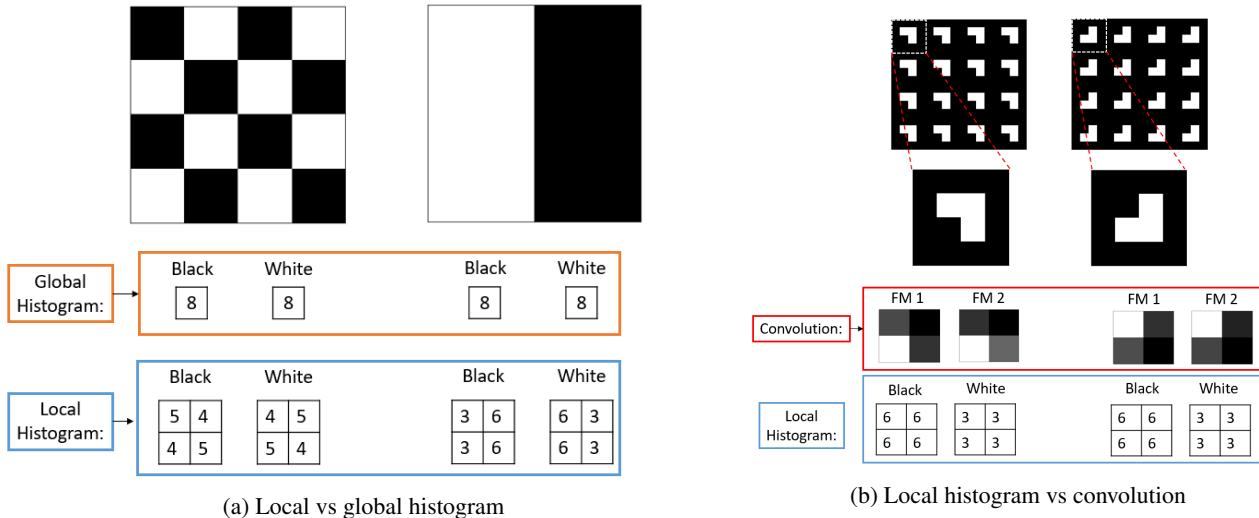


Figure 2: Toy 4×4 images showing the disadvantages of a global histogram (2a) and convolution operation (2b). On the left in 2a, the two images are distinct textures. If a global histogram is computed, the distribution of white and black pixels is equivalent resulting in no discrimination between the two texture types. On the right in 2b, convolution operations are sensitive to image transformations such as rotations. The two textures shown are the same, but applying filters from a convolutional neural network such as ResNet18 in local areas results in different feature maps (FM). However, a local histogram provides some rotational invariance and learns the same local distribution of pixels for each image.

outperformed several traditional approaches and achieved state-of-the-art results in various tasks such as classification, segmentation and object recognition [16, 18, 19, 24]. Despite the success of deep learning, some works have shown empirically and theoretically that traditional features perform better or comparable to that of deep learning methods in texture analysis [3, 4, 8, 22]. Additionally, these deep learning models cannot model the distribution of values in regions which is essential for texture analysis [35]. Deep architectures require more layers resulting in more parameters to characterize the spatial distribution of features in a CNN as opposed to using a histogram directly.

The proposed solution to address problems with both approaches is a histogram layer for artificial neural networks. The histogram layer is a tool to integrate and utilize the strengths of both methods to maximize texture analysis performance. Histograms are an effective and efficient approach to aggregate information. The selection of the bin centers and widths are crucial for the feature representation. Instead of manually determining these parameters, these parameters are estimated through backpropagation. Radial basis functions (RBFs) are used as the histogram binning operation to allow for the gradient information to flow through the network. The contributions of this work are:

- This is the first localized histogram layer for texture analysis enabling the network to aggregate features while maintaining spatial information.

- The bin centers and widths of the histogram are estimated through backpropagation.
- The proposed histogram layer will be less sensitive to image transformations and noise than previous deep learning approaches by accounting for ambiguity and outliers in the data through “soft” assignments to each bin.

2. Related Work

Deep Learning for Texture Analysis Deep learning has been used for texture applications [20, 8]. Attempts to combine neural and traditional features into deep learning architectures have shown success [30, 38, 36, 31], but the traditional features can not be updated through this process. Also, some have tried to emulate handcrafted features via the network design [6, 9, 26] but have run into issues including high computational costs and a decrease in texture analysis performance [20].

Another approach for texture analysis is encoding layers to aggregate the features extracted by the network [11, 42, 33, 39]. As noted by Liu et al., these methods have primarily focused on transfer learning approaches but convolutional neural network (CNN) features are sensitive to image transformations [21, 23] such as rotations as shown in Figure 2. The histogram layer will be more robust than previous methods encoding methods due to “soft” binning assignments that are less sensitive to ambiguity and outliers in

the feature maps. This layer can also be jointly trained with the convolutional layers to influence the features learned by the network.

Pooling Operations Common components of deep learning frameworks are pooling layers. Pooling layers reduce the size of the feature maps resulting in fewer parameters, retain spatial relationships (if not global) and provide some translational invariance [15]. However, these pooling layers make assumptions about the data. Pooling layers can be viewed as histograms with a single bin. For example, max pooling captures the highest feature values and average pooling computes the mean of each descriptor. The statistics captured by these “single bin” histograms will not be optimal for every dataset. For example, some data types (such as synthetic aperture sonar imagery) are plagued with difficult-to-remove speckle noise [1]. The use of min or max pooling will tend to propagate noise values as opposed to more informative values.

Also, many pooling operations (i.e., max pooling) only backpropagate the error through certain locations resulting in a saturation issue that slows learning [41]. The proposed histogram layer will retain the advantages of standard pooling operations but will learn the bin centers and widths necessary to aggregate the features of the data throughout the data distribution. The proposed histogram layer will also be robust to outliers in the data. If a value is far from each bin center, the contribution of the outlier will be negligible. Also, the proposed histogram layer also provides normalization of the features because the contribution of each descriptor for each bin is between the ranges of 0 and 1.

Previous Histogram Layers In the literature, other histogram layers were proposed for applications other than texture analysis. The first histogram layer was developed for semantic segmentation and object detection [37] by Wang, et al. The histogram operation was completed using a linear basis function to backpropagate the error to learn bin centers and widths. Wang et al.’s histogram layer has a convenient property in that it is implemented using pre-existing layers. The second histogram layer was developed for steganalysis [32] and the histograms were modeled using RBFs. Sedighi and Fridich did not update the bin centers and widths, but these values were fixed to simulate the submodels of the projection spatial rich model (PSRM) [17].

The histogram layer proposed in this work inherits properties from each of these models, but also incorporates novel aspects for texture analysis. The histogram layer will use RBFs to represent the histogram structure and this will provide smooth functions to update the bin centers and widths of the model. There are three key differences between our histogram layer and its predecessors. 1) Each of the previous approaches constructed global histograms. Spatial re-

lationships are important in applications involving texture [27, 34] as shown in Figure 2 and a localized approach will retain this information. 2) The number of bins is varied as opposed to the previous methods that used only a single bin number. 3) The histogram layer can be placed anywhere in a network and is stackable.

3. Proposed Histogram Layer

Binning operation Motivated by [32], histogram bins can be modeled with RBFs. The means of the RBFs (μ_{bk}) serve as the location of each bin (i.e., bin centers) while the bandwidth (γ_{bk}) controls the spread of each bin (i.e., bin widths). The normalized frequency count, Y_{rckk} , is computed with a sliding window of size $S \times T$ and the binning operation for a histogram value in the k^{th} channel of the input x is defined as:

$$Y_{rckk} = \frac{1}{ST} \sum_{s=1}^S \sum_{t=1}^T e^{-\gamma_{bk}^2(x_{r+s,c+t,k} - \mu_{bk})^2} \quad (1)$$

where r and c are spatial dimensions of the histogram feature maps. The process of aggregating the feature maps is shown in Figure 3. The histogram layer supports end-to-end learning through backpropagation to update the bin centers and widths. The details and derivation of the update equations are found in Appendix A.

Implementation The histogram layer is implemented using commonly used pre-existing layers as shown in Figure 4. As done in [42, 39], a $1 \times 1 \times K$ convolution is used to reduce the number of input feature maps (a channel-wise pooling operation) where K is the new dimensionality of the feature maps. After the dimensionality reduction, the binning process starts by first assigning each feature value to every bin center (subtracting μ_{bk}). The centering of the features to each bin is calculated by applying a $1 \times 1 \times B$ convolution to each feature map. The weights in the convolution kernels fixed to 1 and each bias serves as the learnable bin centers.

After the features are assigned to the bins, the centered features are then multiplied by the bandwidth (γ_{bk}) to incorporate the spread of the features for each bin. The incorporation of the spread of each bin is also computed by applying a $1 \times 1 \times B$ convolution to each feature map with the weights serving as the learnable bin widths and fixing the biases to be 0. The contribution to each bin is calculated through RBF activation functions in Equation 1. The contribution of each feature to every bin is between 0 and 1. The contributions of features in local spatial regions are then counted through average pooling to compute the normalized frequency count of features belonging to each bin.

4. Experimental Procedure

Datasets Three texture datasets were investigated: Describable Texture Dataset (DTD) [10], a subset of Materials in

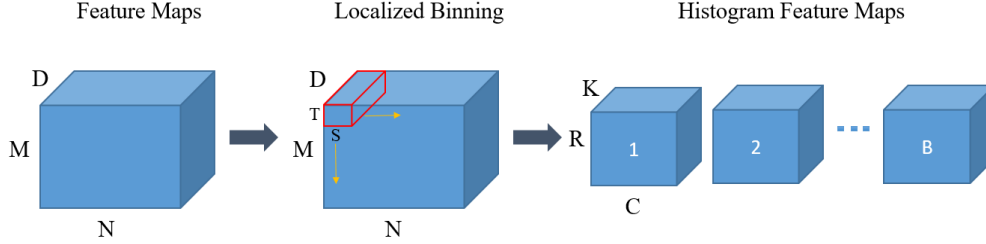


Figure 3: Visualization of localized histogram operation. For the histogram layer, the input is D feature maps with spatial dimensions of $M \times N$. The normalized frequency count, Y_{rckb} , can be computed with a sliding window of size $S \times T$ resulting in B histogram feature maps of size $R \times C \times K$ where B corresponds to the number of bins, R , C , and K are the resulting output dimensions after binning the feature maps.

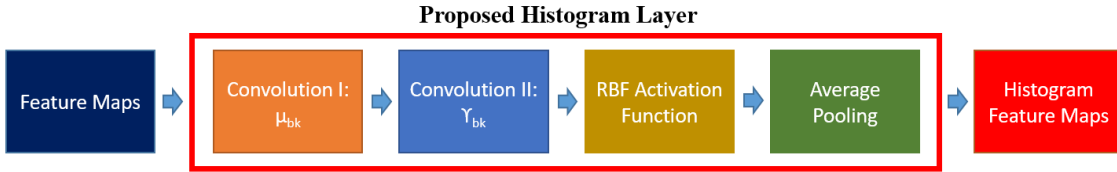


Figure 4: Histogram layer implementation using pre-existing layers.

Context (MINC-2500) [5], and an extension of the ground terrain in outdoor scenes (GTOS-mobile) [39]. For DTD and MINC-2500, the published training and testing splits were used in each experiment (five and ten folds for DTD and MINC-2500 respectively). The ResNet50 architecture was used as the baseline model for these DTD and MINC-2500 while ResNet18 was used for GTOS-mobile [39]. GTOS-mobile only has a single training and test split. GTOS-mobile contains images for different resolutions (256×256 , 384×384 , and 512×512) but only single-scale experiments using 256×256 images were performed in this work.

Architectures Two pre-trained ResNet models, ResNet18 and ResNet50, were used as the baseline for the convolutional features. A comparison is made between different encoding layers for each version of ResNet: 1) global average pooling (GAP), 2) Deep Texture Encoding Network (DeepTEN) [42], 3) Deep Encoding Pooling (DEP) [39], and 4) our HistRes_ B where B is the number of bins. Additionally, the number of bins was varied to investigate the effects of adding additional histogram feature maps to the network. The kernel size for the histogram was 4 by 4 with a stride of 2 to produce 2×2 local feature maps.

Training Details A similar training procedure from [39] was used in this work. For each dataset, the image is resized to 256×256 and a random crop of 80 to 100 % of the image was extracted with a random aspect ratio of $3/4$ to $4/3$. The

crop was then resized to 224×224 and the images were normalized by subtracting the per channel mean and dividing by the per channel standard deviation. A random horizontal flip ($p = .5$) was also added for data augmentation. The training settings for each network were the following: batch size of 64, cross-entropy loss function, SGD with momentum ($\alpha = .9$), learning rates decay every 10 epochs by a factor of .1 and training is stopped after 30 epochs. The initial learning rates for the newly added and pre-trained layers were .01 and .001 respectively.

For the channel-wise pooling, the value of K was selected so that the number of features from the global average pooling and the histogram layer was equal in order to leverage the contribution of texture, spatial and orderless convolutional features. For Resnet18, the number of feature maps was reduced from 512 to 32, 16, and 8 for HistRes_4, HistRes_8, and HistRes_16 respectively. For Resnet50, the number of feature maps was reduced from 2048 to 128, 64, and 32 for HistRes_4, HistRes_8, and HistRes_16 respectively. The bin centers and widths were initialized to values sampled uniformly between $\left(\frac{-1}{\sqrt{BK}}, \frac{1}{\sqrt{BK}}\right)$.

5. Results

The average test accuracy of each model is reported in Table 1. Overall, the histogram model performed better or comparably than GAP, DeepTEN, or DEP. For DTD, each model performed comparably. A reason for this is that a majority of the DTD dataset contains images with homogenous

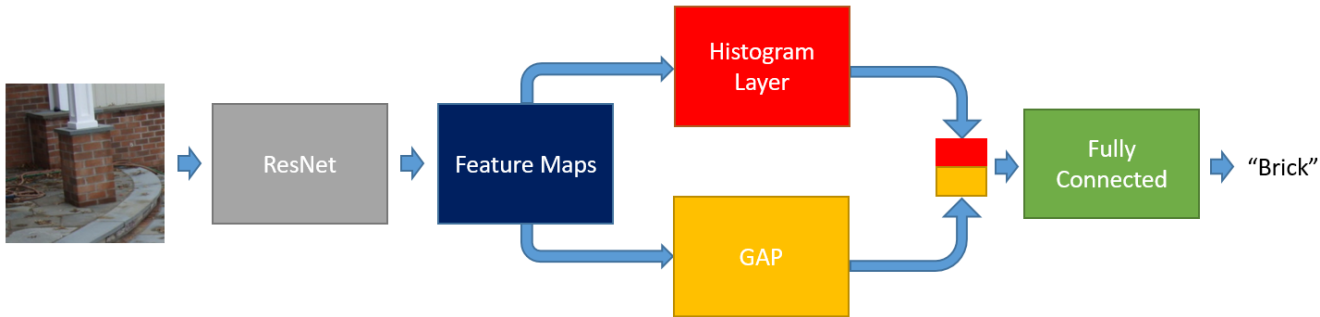
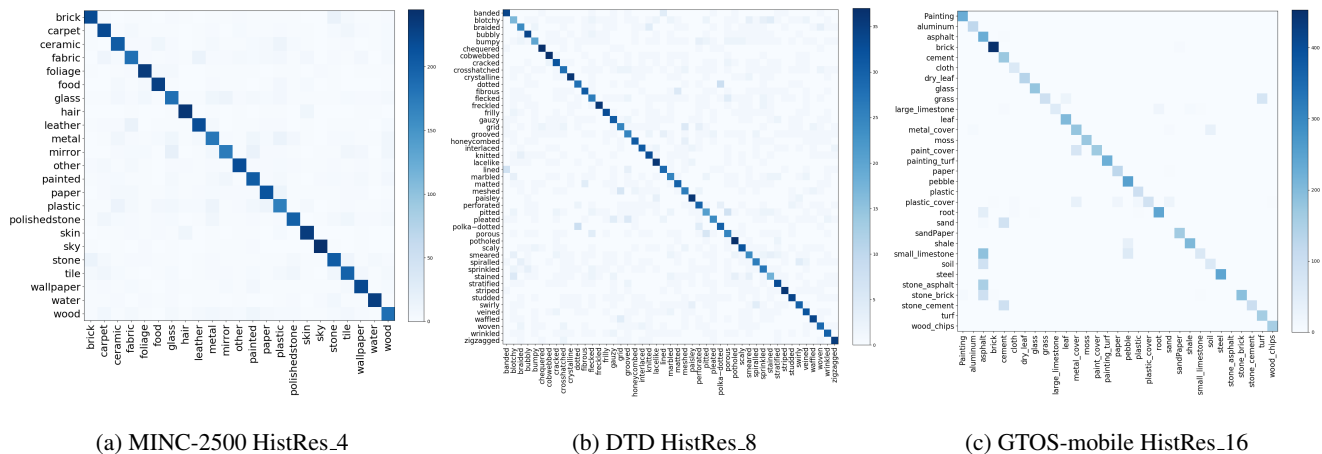


Figure 5: Histogram Layer for ResNet with B bins (HistRes- B). The convolutional features from the model are passed into the global average pooling (GAP) and histogram layer to capture texture, spatial and orderless convolutional features. The features are then concatenated together before being fed into a fully connected layer for classification.

Model	Dataset	ResNet GAP	DeepTEN	DEP	HistRes-4	HistRes-8	HistRes-16
ResNet50	DTD	73.27±0.99%	69.6%	73.2%	73.03±1.05%	73.23±1.20%	73.21±0.80%
ResNet50	MINC-2500	83.38±0.56%	80.4%	82.0%	83.42±0.48%	83.13±0.43%	83.30±0.42%
ResNet18	GTOS-mobile	78.03%	74.22%	76.07%	78.90%	78.77%	79.67%

Table 1: Test accuracy of each encoding method. The results for DeepTEN and DEP are reported from [42] and [39]. For our experiments, we average our results for each data split and show a 1-standard deviation to show the stability of our method (GTOS-mobile only has a single train and test split). The baseline model of ResNet with global average pooling (GAP) is compared with DeepTEN, DEP, and our new histogram model with 4, 8, and 16 bins (HistRes-4, HistRes-8, and HistRes-16 respectively). The result with the best average is bolded.



(a) MINC-2500 HistRes-4

(b) DTD HistRes-8

(c) GTOS-mobile HistRes-16

Figure 6: Average confusion matrices of best performing histogram models for the three texture datasets: MINC_2500 [5] HistRes-4 (6a), HistRes-8 (6b), and HistRes-16 (6c). Each HistRes model performs well across the different datasets.

textures and local information retained by the histogram layer does not provide significant additional information. However, when compared to DeepTEN, a method that focuses on orderless texture information, the addition of spatial information provided by the proposed histogram layer provides improved performance.

For MINC-2500 and GTOS-mobile, most images have

the texture of interest in local regions of the image. The histogram model performed the best out of the other encoding approaches demonstrating the effectiveness of retaining spatial and texture information in the histogram layer. The DEP network also retains both spatial and texture information, but each HistRes- B achieved better accuracy than the DEP model. In Figure 6, the confusion matrices for the

best performing histogram models are shown. Each model performs well across the different classes demonstrating the effectiveness of including the histogram features.

The histogram layer improves performance when compared with the base convolutional network of ResNet18 and ResNet50 (ResNetGAP). Convolutional layers can only capture local, correlated features in the data. For texture analysis, it is important to not only capture local relationships but also learn the distribution of features. Also, the histogram layer is able to learn the distribution of features while being invariant to image transformations such as translation and rotation. As shown in the table, this additional information improved performance for each dataset except DTD, but the HistRes models still achieved comparable performance.

In future works, the histogram layer can be used to further improve performance by making modifications to the implementation. The histogram layer was added at the end of the network, but it may be more advantageous to learn texture information earlier in the network. Previous histogram based features used lower level features (e.g., edges) and learning histograms of convolution features earlier in the network may exploit more texture information. Additionally, changing the scale of the histogram layer may also improve performance. The histogram layer has a window size of 4x4 to produce 2x2 local feature maps. It is difficult to estimate the distribution of local areas with only 16 samples (4x4 windows contain 16 feature values). Increasing the local region of the histogram layer will lead to better estimations of the distributions of each feature map and possibly increase texture analysis performance. Also, adding multiple histogram layers in a network may also improve texture representation since standard neural networks cannot capture this information.

6. Conclusion

In this work, we presented a new layer for deep neural networks, a histogram layer. The histogram layer learns the distribution of features while also maintaining spatial information. This new element can also be used for other architecture besides ResNet and also used in other applications where texture is important [20]. We provide three contributions in this paper: 1) first localized histogram layer for deep neural networks for texture analysis, 2) the bin centers and widths are estimated through the backpropagation of errors to learn the distribution of features, and 3) the histogram layer is robust to outliers by assigning each feature value to every bin based off the distance to each center.

A. Backpropagation

Since the RBFs are used in place of the standard histogram operation, the bin centers and widths can be updated

via backpropagation. Each k^{th} channel of the input x is binned by the histogram in local spatial regions and stored in the r^{th} row and c^{th} column of the output of the histogram layer, Y_{rcbk} . The gradients of the histogram layer with a window size of $S \times T$ are computed by:

$$\frac{\partial Y_{rcbk}}{\partial \mu_{bk}} = \frac{2}{ST} \sum_{s=1}^S \sum_{t=1}^T e^{-\gamma_{bk}^2 (x_{r+s,c+t,k} - \mu_{bk})^2} \times \gamma_{bk}^2 (x_{r+s,c+t,k} - \mu_{bk}) \quad (2)$$

$$\frac{\partial Y_{rcbk}}{\partial \gamma_{bk}} = \frac{-2}{ST} \sum_{s=1}^S \sum_{t=1}^T e^{-\gamma_{bk}^2 (x_{r+s,c+t,k} - \mu_{bk})^2} \times \gamma_{bk} (x_{r+s,c+t,k} - \mu_{bk})^2 \quad (3)$$

where $\frac{\partial Y_{rcbk}}{\partial \mu_{bk}}$ and $\frac{\partial Y_{rcbk}}{\partial \gamma_{bk}}$ are partial derivatives of Y_{rcbk} with respect to the bin centers and widths of the histogram. In [32], the tails of the RBFs were set to 1 resulting in the gradient becoming zero if the feature map value is outside of every bin centers range. In our histogram layer, the gradients are a function of the distance between the feature map value and the bin centers. The gradient contribution from a feature map value will be small if it is far away each bin center (i.e., outliers).

References

- [1] A. Abu and R. Diamant. Robust image denoising for sonar imagery. In *2018 OCEANS-MTS/IEEE Kobe Techno-Oceans (OTO)*, pages 1–5. IEEE, 2018.
- [2] D. T. Anderson, K. E. Stone, J. M. Keller, and C. J. Spain. Combination of anomaly algorithms and image features for explosive hazard detection in forward looking infrared imagery. *IEEE Journal of Selected Topics in Applied Earth Observations and Remote Sensing*, 5(1):313–323, 2012.
- [3] S. Basu, M. Karki, S. Mukhopadhyay, S. Ganguly, R. Nemani, R. DiBiano, and S. Gayaka. A theoretical analysis of deep neural networks for texture classification. In *2016 International Joint Conference on Neural Networks (IJCNN)*, pages 992–999. IEEE, 2016.
- [4] S. Basu, S. Mukhopadhyay, M. Karki, R. DiBiano, S. Ganguly, R. Nemani, and S. Gayaka. Deep neural networks for texture classification—a theoretical analysis. *Neural Networks*, 97:173–182, 2018.
- [5] S. Bell, P. Upchurch, N. Snavely, and K. Bala. Material recognition in the wild with the materials in context database. In *Proceedings of the IEEE conference on computer vision and pattern recognition*, pages 3479–3487, 2015.
- [6] J. Bruna and S. Mallat. Invariant scattering convolution networks. *IEEE transactions on pattern analysis and machine intelligence*, 35(8):1872–1886, 2013.
- [7] G. Castellano, L. Bonilha, L. Li, and F. Cendes. Texture analysis of medical images. *Clinical radiology*, 59(12):1061–1069, 2004.

- [8] P. Cavalin and L. S. Oliveira. A review of texture classification methods and databases. In *2017 30th SIBGRAPI Conference on Graphics, Patterns and Images Tutoriais (SIBGRAPI-T)*, pages 1–8. IEEE, 2017.
- [9] T.-H. Chan, K. Jia, S. Gao, J. Lu, Z. Zeng, and Y. Ma. Pcanet: A simple deep learning baseline for image classification? *IEEE transactions on image processing*, 24(12):5017–5032, 2015.
- [10] M. Cimpoi, S. Maji, I. Kokkinos, S. Mohamed, , and A. Vedaldi. Describing textures in the wild. In *Proceedings of the IEEE Conf. on Computer Vision and Pattern Recognition (CVPR)*, 2014.
- [11] M. Cimpoi, S. Maji, and A. Vedaldi. Deep filter banks for texture recognition and segmentation. In *Proceedings of the IEEE conference on computer vision and pattern recognition*, pages 3828–3836, 2015.
- [12] C. Curio, J. Edelbrunner, T. Kalinke, C. Tzomakas, and W. Von Seelen. Walking pedestrian recognition. In *Proceedings 1999 IEEE/IEEEJ/ISAI International Conference on Intelligent Transportation Systems (Cat. No. 99TH8383)*, pages 292–297. IEEE, 1999.
- [13] N. Dalal and B. Triggs. Histograms of oriented gradients for human detection. In *international Conference on computer vision & Pattern Recognition (CVPR’05)*, volume 1, pages 886–893. IEEE Computer Society, 2005.
- [14] H. Frigui and P. Gader. Detection and discrimination of land mines in ground-penetrating radar based on edge histogram descriptors and a possibilistic k -nearest neighbor classifier. *IEEE Transactions on Fuzzy Systems*, 17(1):185–199, 2008.
- [15] I. Goodfellow, Y. Bengio, and A. Courville. *Deep Learning*. MIT Press, 2016. <http://www.deeplearningbook.org>.
- [16] K. He, X. Zhang, S. Ren, and J. Sun. Deep residual learning for image recognition. In *Proceedings of the IEEE conference on computer vision and pattern recognition*, pages 770–778, 2016.
- [17] V. Holub and J. Fridrich. Random projections of residuals for digital image steganalysis. *IEEE Transactions on Information Forensics and Security*, 8(12):1996–2006, 2013.
- [18] A. Krizhevsky, I. Sutskever, and G. E. Hinton. Imagenet classification with deep convolutional neural networks. In *Advances in neural information processing systems*, pages 1097–1105, 2012.
- [19] M. Liang and X. Hu. Recurrent convolutional neural network for object recognition. In *Proceedings of the IEEE conference on computer vision and pattern recognition*, pages 3367–3375, 2015.
- [20] L. Liu, J. Chen, P. Fieguth, G. Zhao, R. Chellappa, and M. Pietikäinen. From bow to cnn: Two decades of texture representation for texture classification. *International Journal of Computer Vision*, 127(1):74–109, 2019.
- [21] L. Liu, J. Chen, G. Zhao, P. Fieguth, X. Chen, and M. Pietikäinen. Texture classification in extreme scale variations using ganet. *IEEE Transactions on Image Processing*, 2019.
- [22] L. Liu, P. Fieguth, Y. Guo, X. Wang, and M. Pietikäinen. Local binary features for texture classification: Taxonomy and experimental study. *Pattern Recognition*, 62:135–160, 2017.
- [23] L. Liu, P. Fieguth, X. Wang, M. Pietikäinen, and D. Hu. Evaluation of lbp and deep texture descriptors with a new robustness benchmark. In *European Conference on Computer Vision*, pages 69–86. Springer, 2016.
- [24] J. Long, E. Shelhamer, and T. Darrell. Fully convolutional networks for semantic segmentation. In *Proceedings of the IEEE conference on computer vision and pattern recognition*, pages 3431–3440, 2015.
- [25] D. G. Lowe et al. Object recognition from local scale-invariant features. In *iccv*, volume 99, pages 1150–1157, 1999.
- [26] J. M. Malof, J. Bralich, D. Reichman, and L. M. Collins. Improving the histogram of oriented gradient feature for threat detection in ground penetrating radar by implementing it as a trainable convolutional neural network. In *Detection and Sensing of Mines, Explosive Objects, and Obscured Targets XXIII*, volume 10628, page 106280D. International Society for Optics and Photonics, 2018.
- [27] T. Ojala and M. Pietikäinen. Texture classification, machine vision, and media processing unit. *University of Oulu, Finland*, 2004.
- [28] T. Ojala, M. Pietikäinen, and D. Harwood. Performance evaluation of texture measures with classification based on kullback discrimination of distributions. In *Proceedings of 12th International Conference on Pattern Recognition*, volume 1, pages 582–585. IEEE, 1994.
- [29] T. Ojala, M. Pietikäinen, and T. Mäenpää. Multiresolution gray-scale and rotation invariant texture classification with local binary patterns. *IEEE Transactions on Pattern Analysis & Machine Intelligence*, (7):971–987, 2002.
- [30] R. Paul, S. H. Hawkins, L. O. Hall, D. B. Goldgof, and R. J. Gillies. Combining deep neural network and traditional image features to improve survival prediction accuracy for lung cancer patients from diagnostic ct. In *2016 IEEE International Conference on Systems, Man, and Cybernetics (SMC)*, pages 002570–002575. IEEE, 2016.
- [31] C.-A. Rivera-Morales, M.-X. Bastidas-Rodríguez, and F.-A. Prieto-Ortiz. Densenet model combined with haralicks hand-crafted features for texture classification. In *2018 IEEE Latin American Conference on Computational Intelligence (LACCI)*, pages 1–6. IEEE, 2018.
- [32] V. Sedighi and J. Fridrich. Histogram layer, moving convolutional neural networks towards feature-based steganalysis. *Electronic Imaging*, 2017(7):50–55, 2017.
- [33] Y. Song, F. Zhang, Q. Li, H. Huang, L. J. O’Donnell, and W. Cai. Locally-transferred fisher vectors for texture classification. In *Proceedings of the IEEE International Conference on Computer Vision*, pages 4912–4920, 2017.
- [34] G. Srinivasan and G. Shobha. Statistical texture analysis. In *Proceedings of world academy of science, engineering and technology*, volume 36, pages 1264–1269, 2008.
- [35] M. Tuceryan and A. K. Jain. Texture analysis. In *Handbook of pattern recognition and computer vision*, pages 235–276. World Scientific, 1993.
- [36] H. Wang, A. C. Roa, A. N. Basavanhally, H. L. Gilmore, N. Shih, M. Feldman, J. Tomaszewski, F. Gonzalez, and

- A. Madabhushi. Mitosis detection in breast cancer pathology images by combining handcrafted and convolutional neural network features. *Journal of Medical Imaging*, 1(3):034003, 2014.
- [37] Z. Wang, H. Li, W. Ouyang, and X. Wang. Learnable histogram: Statistical context features for deep neural networks. In *European Conference on Computer Vision*, pages 246–262. Springer, 2016.
- [38] J. Wu, Z. Lin, and H. Zha. Multi-view common space learning for emotion recognition in the wild. In *Proceedings of the 18th ACM International Conference on Multimodal Interaction*, pages 464–471. ACM, 2016.
- [39] J. Xue, H. Zhang, and K. Dana. Deep texture manifold for ground terrain recognition. In *Proceedings of the IEEE Conference on Computer Vision and Pattern Recognition*, pages 558–567, 2018.
- [40] Y. Yang and S. Newsam. Bag-of-visual-words and spatial extensions for land-use classification. In *Proceedings of the 18th SIGSPATIAL international conference on advances in geographic information systems*, pages 270–279. ACM, 2010.
- [41] D. Yu, H. Wang, P. Chen, and Z. Wei. Mixed pooling for convolutional neural networks. In *International Conference on Rough Sets and Knowledge Technology*, pages 364–375. Springer, 2014.
- [42] H. Zhang, J. Xue, and K. Dana. Deep ten: Texture encoding network. In *Proceedings of the IEEE Conference on Computer Vision and Pattern Recognition*, pages 708–717, 2017.